

Cost estimation relationships of a small scale linear Fresnel reflector

A. Barbón^a, J.A. Sánchez-Rodríguez^a, L. Bayón^{b,*}, C. Bayón-Cueli^c

^a Department of Electrical Engineering, University of Oviedo, Campus of Gijón, Spain

^b Department of Mathematics, University of Oviedo, Campus of Gijón, Spain

^c Polytechnic School of Engineering of Gijón, University of Oviedo, Spain



ARTICLE INFO

Article history:

Received 20 February 2018

Received in revised form

17 August 2018

Accepted 17 September 2018

Available online 20 September 2018

Keywords:

Linear Fresnel reflector

Cost estimating relationship

ABSTRACT

This paper presents a cost estimating relationship (*CER*) of a novel small scale linear Fresnel reflector (*SSLFR*). The *CER* has been developed analyzing in detail the manufacturing processes of the *SSLFR*, its parameters, and the possible sub-components. As a result of this analysis, the *SSLFR* has been divided into 8 sub-components: fixed and mobile structures, movement units, mirror units, secondary reflector system, tracking system, assembly, and foundation. These sub-components are described in detail and designed using Autodesk Inventor, specifying manufacturing materials and processes. The study includes a full stress analysis of the sub-components, considering self weight, snow loads, and wind loads. For each sub-component an estimate of the primary costs is presented and also a relationship between the cost and the geometric parameters of the *SSLFR*. The primary costs considered include material, labor, and tooling costs. A numerical example shows the suitability of the proposed approach.

© 2018 Elsevier Ltd. All rights reserved.

1. Introduction

The growing interest in solar thermal energy is due to several factors: i) The demand of industrial process heat is more than 66% of the total global industrial energy consumption, and 50% of this demand is low-to medium-temperatures ($< 400\text{ }^{\circ}\text{C}$) [1]; ii) Globally, solar thermal energy can provide about 50% of this demand [1]; iii) The demand of heat in the building sector, in the European Union (EU), is more than 40% of the final energy consumption [2]; iv) European standards require new buildings to obtain from solar sources part of the energy needed for the hot water service, depending on the climate zone and on the total hot water demand [2]; v) Solar thermal energy can provide hot water and steam (temperature range of up to $400\text{ }^{\circ}\text{C}$) needed for domestic water heating, heating of buildings, pasteurisation, sterilisation, washing, boiling, etc. [1]. Therefore, solar thermal energy can fulfill a substantial amount of heat demand in the building and industrial sectors.

Three different solar thermal technologies can be used in the building and industrial sectors: solar air collectors, solar non-concentrating collectors (flat-plate collector (*FPC*) and evacuated tube collector (*ETC*)), and solar concentrating collectors (parabolic

trough collector (*PTC*), parabolic dish reflector (*PDR*), and linear Fresnel reflector (*LFR*)).

This paper is focused on small scale linear Fresnel reflectors (*SSLFRs*). These systems have a wide range of applications in buildings and in the industrial sector. *SSLFRs* are used in domestic water heating (Sultana et al. [3,4], Mokhtar et al. [5]), in the heating/cooling of buildings (Bermejo et al. [6], Pino et al. [7], Serag-Eldin [8]), in the absorption air cooled Solar-GAX cycle (Velázquez et al. [9]), and also in industrial applications (Singh [10], Häberle et al. [11], Rawlins and Ashcroft [12]). Recently, a paper has been published on the use of a *SSLFR* as sunlight collector in a fiber daylighting system [13].

In this paper we present constructive details and a cost estimation of a novel *SSLFR* with triple movement that allows to maximize the absorption of solar energy [14], reduce the space needed for its installation [15] and reduce the separation between several *SSLFR* installed on the same roof.

Different cost estimation methods have been proposed in the literature [16]: intuitive, analogical, parametric, and analytical methods. The intuitive method is based on using the past experience. The analogical method evaluates the cost of a product comparing it with the cost of other already existing products. The analytical method breaks down the work into elementary tasks and parts. Finally, the parametric method relates the cost of a product with the parameters that define it.

There are three well-recognized parametric cost estimation

* Corresponding author.

E-mail address: bayon@uniovi.es (L. Bayón).

Nomenclature			
A	Mirror field area (m^2)	k^{Se}	Cost parameter of the sensors (€)
A_{CR}	Area of the cavity receiver (m^2)	$k^{shaft\ Mi}$	Cost parameter of the shaft mirror ($\text{€}/m$)
A_{GC}	Area of the glass covering (m^2)	$k^{shaft\ SRS}$	Cost parameter of the shaft of the secondary reflector system ($\text{€}/m$)
A_I	Area of the isolation (m^2)	L_{AT}	Length of the absorber tube (m)
A_{PC}	Area of the protective casing (m^2)	L_{FS}	Length of the fixed structure (m)
A_{frame}	Area of a frame (m^2)	L_{MS}	Length of the mobile structure (m)
A_{mirror}	Area of a mirror (m^2)	L_M	Length of the mirrors (m)
a	Configuration constant	L_{SRSS}	Length of the secondary reflector system structure (m)
C_A	Primary cost of the assembly (€)	L_a	Length of the single absorber tube (m)
C_F	Primary cost of the foundation (€)	L_i	Position of i – th mirror ($0 < i < n$) (m)
C_{FS}	Primary cost of the fixed structure (€)	L_{rail}	Length of the rail support (m)
C_{MS}	Primary cost of the mobile structure (€)	L_{shaft}	Length of the shaft of the a mirror (m)
C_{MIS}	Primary cost of the movement system (€)	n	Number of mirrors at each side of the central mirror
C_{MoS}	Primary cost of the mirror system (€)	V_F	Volume of the foundation (m^3)
C_{SRS}	Primary cost of the secondary reflector system (€)	W_{AT}	Weight of the absorber tube (kg)
C_T	Total cost of the SSLFR (€)	W^U	Weight unitario (kg/m)
C_{TS}	Primary cost of the tracking system (€)	W_M	Width of the mirrors (m)
D	Diameter of the absorber tube (m)	W_{FS}	Weight of the fixed structure (kg)
d	Separation between two consecutive mirrors (m)	W_{MS}	Weight of the mobile structure (kg)
f	Height of the receiver (m)	W_{SRSS}	Weight of the secondary reflector system structure (kg)
k^A	Cost parameter of the assembly (€)	W_{ai}	Width illuminated on the absorber by the i -th by mirror (m)
k^{AT}	Cost parameter of the absorber tube ($\text{€}/kg$)	α_i	Angle between the vertical at the focal point and the line connecting the centre point of each mirror to the focal point ($^\circ$)
k^C	Cost parameter of the controller (€)	β_a	Angle between the absorber tube and the horizontal plane ($^\circ$)
k^{CR}	Cost parameter of the receiver cavity ($\text{€}/m^2$)	β_i	Tilt of i – th mirror ($^\circ$)
k^F	Cost parameter of the foundation ($\text{€}/m^3$)	β_M	Angle between the mirror axis and the horizontal plane ($^\circ$)
k^{GC}	Cost parameter of the glass covering ($\text{€}/m^2$)	θ_i	Angle between the normal to the mirror and the angle of incidence of the sun ($^\circ$)
k^I	Cost parameter of the insulation ($\text{€}/m^2$)	θ_l	Longitudinal incidence angle ($^\circ$)
k^{MD}	Cost parameter of the stepper motor and stepper motor driver (€)	θ_t	Transversal incidence angle ($^\circ$)
k^{MiU}	Cost parameter of the mirror unit ($\text{€}/unit$)	θ_z	Zenith angle of the Sun ($^\circ$)
k^{MoU}	Cost parameter of the movement unit ($\text{€}/unit$)		
k^{PC}	Cost parameter of the protective casing ($\text{€}/m^2$)		
k^R	Cost parameter rail support ($\text{€}/m$)		
k^{St}	Cost parameter structure ($\text{€}/kg$)		
k^{frame}	Cost parameter of the frame ($\text{€}/m^2$)		
k^{mirror}	Cost parameter of the mirror ($\text{€}/m^2$)		
$k^{pinion\ gear}$	Cost parameter of the pinion gear ($\text{€}/pinion\ gear$)		

methods: method of scales, statistical parametric cost estimation model, and cost estimating relationship (CER). The method of scales is very simple and relates the cost to the most significant technical parameter of the product. The statistical parametric cost estimation model analyzes, using statistical techniques, the past experience with the manufacturing process [17].

The CER method, also known as cost estimation formulae method, relates the cost of a product with a limited number of parameters.

The purpose of this work is to develop a cost estimating relationship for a small scale linear Fresnel reflector. Using this CER, the primary cost of an SSLFR-based installation can be calculated and compared with that of other solar thermal technologies.

The paper is organized as follows. In Section 2 the basic definitions are presented, describing the parameters and the components of the SSLFR. Section 3 details the adopted methodology. A numerical example is presented in Section 4. Finally, Section 5 summarizes the main conclusions of this study.

2. Basic definitions

A small scale linear Fresnel reflector (SSLFR) consists of a row of

mirrors that focus incident solar radiation on an absorber tube located at a common focal line of the mirrors. The row of mirrors is located at the base of the SSLFR and the absorber tube runs longitudinally above them. The concentrated solar energy is transferred through the absorber tube into some thermal fluid.

2.1. Description of the components of an SSLFR

This subsection outlines the material and component specifications of an SSLFR. An SSLFR has the configuration of a 'conventional' central LFR [14]. Fig. 1 shows a picture of an SSLFR prototype that has been manufactured in a vocational training school (CIFP-Mantenimiento y Servicios a la Producción) in La Felguera, Asturias, Spain. This prototype has been patented (see Ref. [18]).

An SSLFR, as shown in Fig. 2, is composed of six main blocks: fixed structure (1), mobile structure (2), primary reflector system (4), secondary reflector system (3), transmission systems (7), and tracking system (8). The primary reflector system is made up of multiple mirrors mounted on specially designed frames (5). The secondary reflector system (see Fig. 3) is composed of: absorber tube (9), receiver cavity (10), insulation (11), and glass covering (12). The absorber tube is encased in a receiver cavity to reduce



Fig. 1. Prototype.

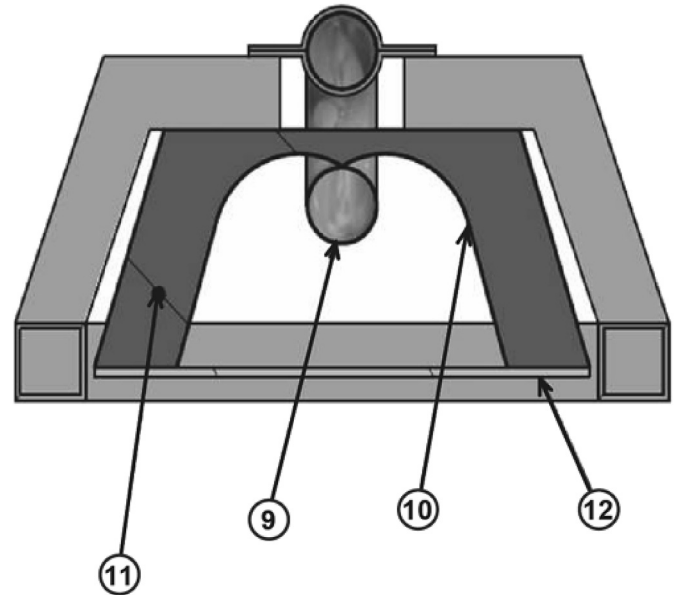


Fig. 3. Secondary reflector system.

The mobile structure can be rotated on the east-west axis. The primary reflector system can be rotated on the north-south axis so as to follow the sun's movement. Finally, the secondary reflector system can also be rotated on the east-west axis.

2.2. SSLFR parameters

This section describes the parameters that determine the transversal and longitudinal behaviour of the SSLFR [14,19]. Considering an SSLFR aligned horizontally and aligned in a north-south orientation, the angle of incidence of solar radiation will be calculated in two projection planes (see Ref. [20]): the transversal incidence angle (θ_t) and the longitudinal incidence angle (θ_l).

The parameters used in the transversal study are as follows: n is the number of mirrors at each side of the central mirror (the total number of mirrors of the SSLFR is $2n + 1$), W_M is the mirror width, d is the separation between two consecutive mirrors, L_i is the position with respect to the central mirror of the i -th mirror, β_i is the mirror tilt of i -th mirror, α_i is the angle between the vertical at the focal point and the line connecting the centre point of each mirror to the focal point, D is the diameter of the absorber tube, and f is the height of the receiver. The parameters used in the longitudinal study are as follows: β_M is the angle between the mirror axis and the horizontal plane, β_a is the angle between the absorber tube and the horizontal plane, θ_z is the zenithal solar angle, L_M is the mirror length, and L_a is the total length of the absorber tube. The mirror field width (W) can be calculated as:

$$W = 2 \cdot n \cdot (W_M + d) + W_M \tag{1}$$

Using a method known as 'Mathur's method' ([21,22]), we calculate the appropriate value of the shift between adjacent mirrors such that shading and blocking of reflected rays are avoided for a transversal incidence angle between -22.5° and 22.5° . The relationship between W_M and d is given by:

$$d = 0.075 \cdot W_M \tag{2}$$

The mirror field area (A) can be calculated as:

$$A = W \cdot L_M = W_M \cdot L_M \cdot (1 + 2.15 \cdot n) \tag{3}$$

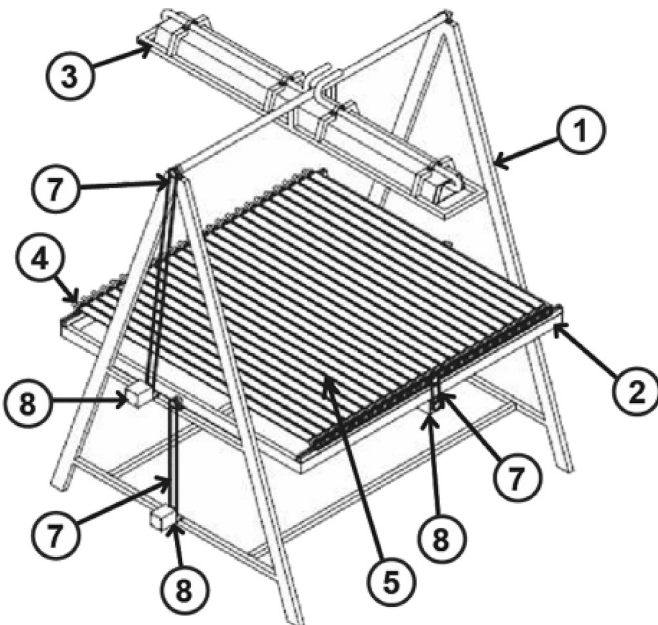


Fig. 2. SSLFR parts.

convective heat losses and specially coated so as to increase the absorption capability of the incident solar radiation. The receiver cavity is sealed with a glass cover and silicon rubber beading. The fixed structure rests on a foundation made for this purpose.

The SSLFR considered makes use of a two axis tracking system.

Different configurations can be studied with our prototype [14]. In this paper, we present a cost analysis of C_9 configuration, where the rays reflected by the mirrors in the longitudinal direction are always vertical for any time of day. Nevertheless, the cost analysis methodology is the same for all configurations.

3. Methodology

A cost estimating relationship (*CER*) can be defined as [23]: “a technique used to estimate a particular cost or price using an established relationship with an independent variable”. A *CER* may be mathematically simple or it may involve complex parametric equations. Usually, the number of parameters used as independent variables is between two and five. The following steps represent the *CER* development process [23]: i) Define the dependent variable; ii) Select independent variables; iii) Select the relationship between the dependent and independent variables.

Fig. 4 shows the graphical abstract of this cost-estimating relationship. This figure first shows the sub-components into which the study was divided. Then, the independent variables related to each sub-component are determined. The next step is to relate these independent variables to the material used to manufacture each sub-component. Finally, the material costs, labour costs and tooling costs are related to each sub-component to obtain the cost of each one of the systems that make up this *SSLFR*. The sum of these costs

will result in the total cost.

3.1. Define the dependent variable

In this work, the *CER* will be used to estimate the cost of one of the possible configurations of an *SSLFR*.

3.2. Select independent variables

As a result of a detailed analysis of the manufacturing processes of the *SSLFR*, its parameters, and the possible sub-components, the *SSLFR* has been divided into 8 sub-components: fixed and mobile structures, movement units, mirror units, secondary reflector system, tracking system, assembly, and foundation. Independent variables are selected from the parameters that characterize these sub-components.

The assumptions made in this study are as follows:

- (i) The study includes a full stress analysis of the sub-components, considering self weight, snow loads, and wind loads. Wind load is proportional to component area and wind speed. All the calculations are carried out considering a wind speed of 100 (km/h) in order to simulate severe weather conditions. Fig. 5 shows an example of the stress analysis generated by Autodesk Inventor.

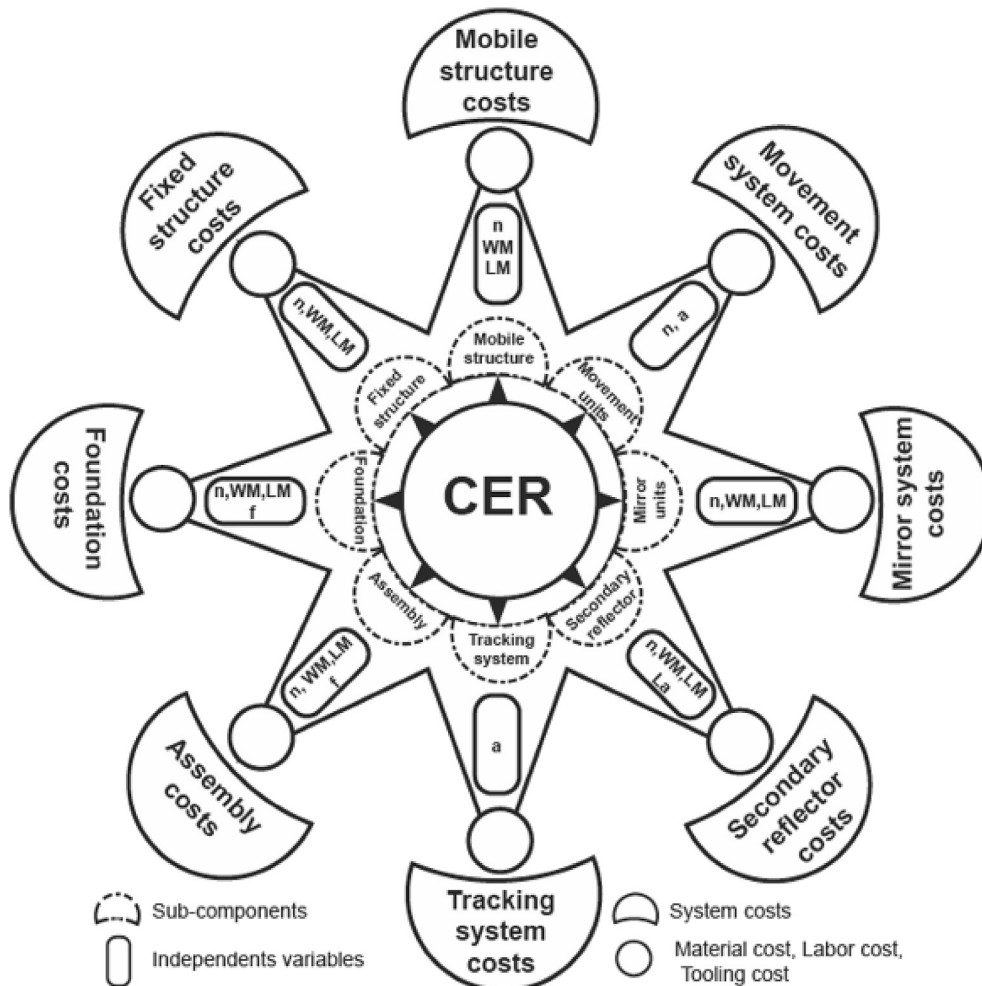


Fig. 4. Cost estimating relationship process.

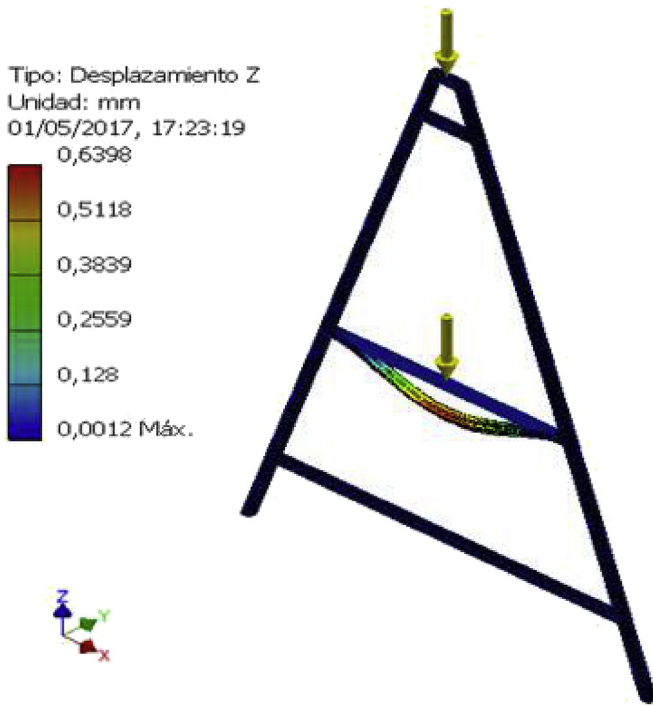


Fig. 5. Stress analysis.

- (ii) The structures are made of steel square or rectangular hollow sections in order to simplify manufacturing and building processes.
- (iii) The range of variation of the dimensions (W_M , L_M , L_a , f , and n) is in accordance with our previous work [24].
- (iv) Structural steel elements are galvanized.
- (v) Structural steel elements are designed as per ANSI/AISC 360-10 considering a life span of 25 years.

The many factors influencing the lineal Fresnel tracking error may be divided into factors related to the structural system, those related to the tracking system, and those related to the installation. With respect to the structural system, these factors are in turn due to the reflector supporting structure, absorber tube supporting structure, and rotation axis position [25]. As to the tracking system, there are factors such as driver accuracy, tracking software algorithm, and deviation in geographic latitude-longitude [25]. With respect to the installation, there is the deviation in geographic North-South orientation. All these errors reduce the efficiency of the SSLFR. In this study, the following elements were taken into consideration:

- (vi) Fixed and mobile structure. In these systems, the tracking error and misalignment are not considered.
- (vii) Primary reflector system. The pivoting point of each mirror coincides with the central point of the mirror; hence, it is always focused on the central point of the absorber tube. The mirrors are flat and specularly reflecting. The mirrors have the same length and width.
- (viii) Transmission systems. The tracking error and misalignment are not considered in these systems.
- (ix) Tracking system. The mobile structure, secondary reflector system, and primary reflector system are perfectly tracked so as to follow the apparent movement of the Sun.
- (x) Considering the SSLFR perfectly aligned in a North-South orientation.

3.2.1. Fixed structure

Fig. 6 shows the fixed structure designed with Autodesk Inventor. The selected dimensions of the steel square hollow sections are: $100 \times 100 \times 3$ (mm).

The cost of the structure depends on the weight of the steel sections and this is proportional to the total length, L_{FS} . According to Fig. 6, L_{FS} is given by:

$$L_{FS} = 2 \cdot W + 4 \cdot \sqrt{\left(\frac{L_M}{2} + f\right)^2 + \left(\frac{L_M}{2}\right)^2} + 2 \cdot L_M + \frac{1}{2} \cdot (2 \cdot L_M) \quad (4)$$

The value adopted for the height of the receiver (f) is 1.5 (m) [24,26], since it provides a good collector optical efficiency. Therefore, Eq. (4) can be expressed as:

$$L_{FS} = 2 \cdot W_M \cdot (1 + 2.15 \cdot n) + 3 \cdot L_M + 4 \cdot \sqrt{2 \cdot \left(\frac{L_M}{2}\right)^2 + 1.5 \cdot L_M + (1.5)^2} \quad (5)$$

The linear weight of the selected steel rectangular hollow sections is $W_{FS}^U = 8.96$ (kg/m) (manufacturer's data). The total weight of the fixed structure is given by:

$$W_{FS} = W_{FS}^U \cdot L_{FS} \quad (6)$$

Therefore, the cost of the fixed structure is determined by the following independent variables: W_M , L_M , and n .

3.2.2. Mobile structure

The mobile structure consists of a steel rectangular hollow section and an installation channel where movement units are located. Fig. 7 shows the mobile structure designed with Autodesk

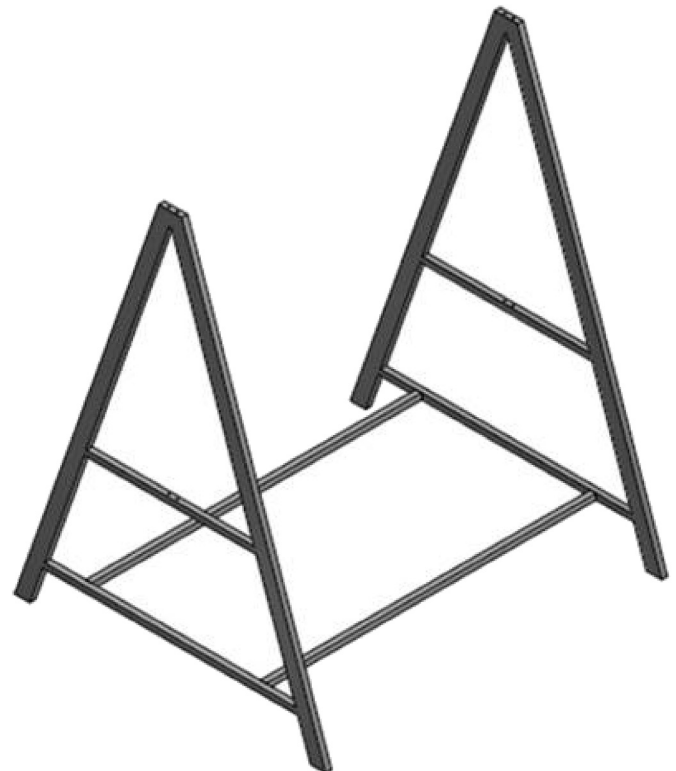


Fig. 6. Fixed structure.

Inventor. The selected dimensions of the steel rectangular hollow section are: $80 \times 40 \times 3$ (mm).

According to Fig. 7, the length of the steel rectangular hollow section (L_{MS}) is given by:

$$L_{MS} = 2 \cdot (W + L_M) = 2 \cdot (W_M \cdot (1 + 2.15 \cdot n) + L_M) \quad (7)$$

The linear weight of the selected steel rectangular hollow section is $W_{MS}^U = 5.19$ (kg/m) (manufacturer's data), and the total weight is given by:

$$W_{MS} = W_{MS}^U \cdot L_{MS} = W_{MS}^U \cdot (2 \cdot (W_M \cdot (1 + 2.15 \cdot n) + L_M)) \quad (8)$$

The installation channel is made of stainless steel. We have selected a standard channel manufactured by Hilti with dimensions 40×40 (mm). The cost is proportional to the total length (L_{rail}) which is given by:

$$L_{rail} = 2 \cdot W = 2 \cdot W_M \cdot (1 + 2.15 \cdot n) \quad (9)$$

Therefore, the cost of the mobile structure is determined by the following independent variables: W_M , L_M and n .

3.2.3. Movement units

The position of the mirrors and the absorber of the SSLFR can be adjusted using three different movements. First, the mirrors can be rotated on the north-south axis, so as to follow the sun's daily movement. This movement requires $2 \cdot n + 1$ movement units. Second, the mirror row can be rotated on the east-west axis. Finally, the receiver can also be rotated on the east-west axis. These movements require 2 additional movement units.

Each movement unit (see Fig. 8) includes: two bearings, two bearing supports, two shafts, a pinion gear, and the proportional part of the roller chain.

Selected elements are as follows. Standard bearing type FAG 7205 B.TVP. Standard pinion gear with 19 tooth, step $3/8$ ", module 3 (mm), and thickness 5 (mm). The bearing support consists of an 82.5 (mm) diameter stainless steel tube with a 20 (mm) wall thickness, and a $78 \times 28 \times 5$ (mm) stainless steel plate. The shaft consists of a 25 (mm) diameter carbon steel bar with a length of 150 (mm). The chain is a standard single strand, riveted, 6 (mm) size, roller chain.

3.2.4. Mirror units

Each mirror unit (see Fig. 9) includes: a mirror, a frame, and a shaft.

The mirror has a thickness of 5 (mm) and is made with low iron content for outdoor use with a minimum reflectivity of 96%. The

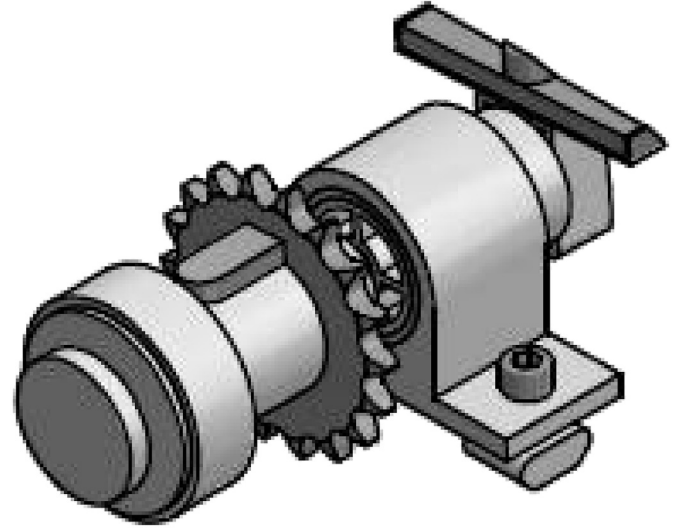


Fig. 8. Movement unit.

mirror is pasted onto the frame using an industrial adhesive. The frame is a 0.8 (mm) thick galvanized steel sheet. The shaft is a $3/4$ " diameter galvanized steel tube that is assembled to the support by stainless steel rivets.

The mirror cost depends on its area (A_{mirror}), which is given by:

$$A_{mirror} = W_M \cdot L_M \quad (10)$$

The frame cost depends also on its area (A_{frame}), which is given by:

$$A_{frame} \approx W_M \cdot L_M \quad (11)$$

The shaft cost depends on its length (L_{shaft}), which is given by:

$$L_{shaft} = L_M \quad (12)$$

Therefore, the cost of the mirror units is determined by the following independent variables: W_M and L_M .

3.2.5. Secondary reflector system

The secondary reflector system (see Fig. 10) includes: the absorber tube, the receiver cavity, insulation, glass covering, structure, protective casing, and a shaft.

Pressure and flow rate of the thermal fluid in the absorber tube



Fig. 7. Mobile structure.

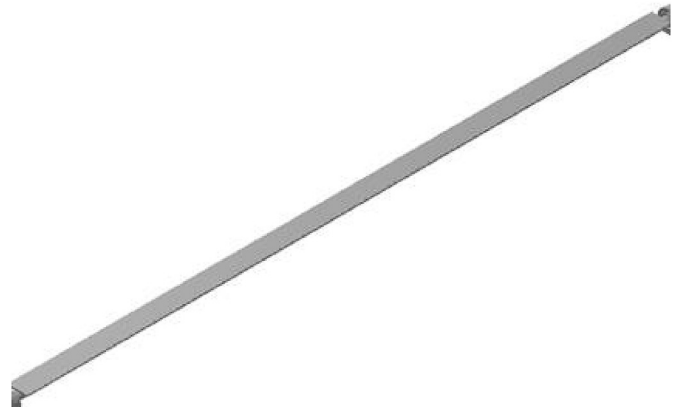


Fig. 9. Mirror unit.

have been taken into account in order to design the elements of this system. The absorber tube is a carbon steel tube, dull black painted, 48.6 (mm) in diameter and 3.68 (mm) thick. The receiver cavity consists of a polished stainless steel sheet 0.6 (mm) thick. Insulation consists of a glass wool 100 (mm) thick. The glass covering is made of a tempered glass 5 (mm) thick. The structure is made of a steel square hollow section with dimensions 40 × 40 × 1.5 (mm). The secondary reflector system is covered with an aluminum sheet 0.6 (mm) thick. The shaft is a 2" diameter galvanized steel tube.

According to Fig. 10, the length of the absorber tube (L_{AT}) is given by:

$$L_{AT} = 2 \cdot L_a \quad (13)$$

The linear weight of the absorber tube is $W_{AT}^U = 4.05$ (kg/m) (manufacturer's data), and the total weight is given by:

$$W_{AT} = W_{AT}^U \cdot L_{AT} = W_{MS}^U \cdot 2 \cdot L_a \quad (14)$$

The cost of the receiver cavity depends on its area (A_{CR}). As the profile curve of the receiver cavity is an involute, its area is given by:

$$A_{CR} \approx L_a \cdot 2 \cdot \sqrt[3]{2} \cdot W_{an \max} \quad (15)$$

where $W_{an \max}$ is the maximum illuminated width on the absorber tube by the n – th mirror. $W_{an \max}$ is given by:

$$W_{an \max} = W_M \cdot [\cos \beta_{n \max} \pm \sin \beta_{n \max} \tan \alpha_n] \quad (16)$$

where α_n is the angle between the vertical at the focal point and the line connecting the centre point of the n – th mirror to the focal point. The sign \pm must be adopted according to the following criteria: – for the left side, and + for the right side. The angle α_n can be calculated as:

$$\alpha_n = \arctan \left[\frac{n \cdot (W_M + d)}{f + D/2} \right] = \arctan \left[\frac{n \cdot 1.075 \cdot W_M}{f + D/2} \right] \quad (17)$$

Therefore, Eq. (15) can be expressed as:

$$A_{CR} \approx L_a \cdot 2 \cdot \sqrt[3]{2} \cdot 1.2 \cdot W_M = 3.40 \cdot L_a \cdot W_M \quad (18)$$

The area of the insulation (A_I) is the same as the area of the receiver cavity:

$$A_I = A_{CR} = 3.40 \cdot L_a \cdot W_M \quad (19)$$

The area of the glass covering (A_{GC}) is given by:

$$A_{GC} \approx L_a \cdot 2 \cdot W_{an \max} \approx L_a \cdot 2 \cdot 1.2 \cdot W_M \approx 2.4 \cdot L_a \cdot W_M \quad (20)$$

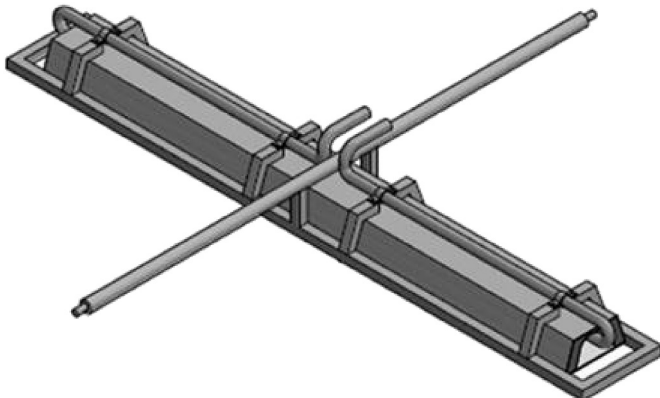


Fig. 10. Receiver system unit.

The length of the steel rectangular hollow section (L_{SRSS}) is given by:

$$L_{SRSS} \approx 3 \cdot (L_a + 2 \cdot W_{an \max}) \approx 3 \cdot (L_a + 2 \cdot 1.2 \cdot W_M) \approx 3 \cdot (L_a + 2.4 \cdot W_M) \quad (21)$$

The linear weight of the selected steel rectangular hollow section is $W_{SRSS}^U = 1.70$ (kg/m), and the total weight is given by:

$$W_{SRSS} = W_{SRSS}^U \cdot L_{SRSS} = W_{SRSS}^U \cdot (L_a + 2.4 \cdot W_M) \quad (22)$$

The area of the protective casing (A_{PC}) is given by:

$$A_{PC} \approx L_a \cdot 2 \cdot \sqrt[3]{2} \cdot 1.2 \cdot W_M = 3.40 \cdot L_a \cdot W_M \quad (23)$$

The length of the shaft ($L_{shaft \ SRS}$) is given by:

$$L_{shaft \ SRS} = W_M \cdot (1 + 2.15 \cdot n) \quad (24)$$

Therefore, the cost of the secondary reflector system is determined by the following independent variables: W_M , L_M , L_a , and n .

3.2.6. Tracking system

The sun position for a tracking system can be calculated using the international Solar Position Algorithm (SPA) [27], whose accuracy is 0.0003°. This error is extremely small from the point of view of solar engineering. Other algorithms have been designed specifically for solar energy applications, with maximum errors of 0.01° [28], 0.008° [29], and 0.0027° [30]. Grena has proposed five new algorithms [31] with similar accuracy. Taking into account the required precision, it is considered that the suitable electric motor is the stepper motor [32,33]. With the right driver, a stepper motor can rotate with a step of 0.006°.

The tracking algorithm is implemented in a controller based on a Raspberry Pi 3 [34,35], due to its low cost, compact size, compatibility and easy interfacing. The Raspberry Pi 3 is a single board computer based on a 900 MHz quad-core ARM Cortex-A7 CPU, with 1 GB RAM, 40 GPIO pins, 4 USB ports, Full HDMI port, Ethernet port, and a Micro SD card slot.

A total of three stepper motors and drivers are required, since the position of the mirrors and the absorber of the SSLFR can be adjusted using three different movements. Each driver supplies appropriate control signals and supply voltage to the associated stepper motor. The system requires additional sensors such as: wind sensor, encoder, limit switches.

3.2.7. Assembly

The cost of the assembly of the sub-components is determined by the following independent variables: W_M , L_M , f , and n . Of these variables, the one that most influences the cost is n , since it defines the number of sub-components.

3.2.8. Foundation

The cost of foundation depends on the soil conditions. As already mentioned, these SSLFRs can be used in domestic water heating, or to provide heating/cooling for buildings. Therefore, roofs are a logical location for SSLFRs [15].

There are four principal types of foundations for ground mounted solar installations: driven piles, helical piles, earth-screws, and ballasted foundations. In this paper we consider pre-cast ballasted foundations, since they are a good option for the installation of SSLFR support structures in roofs.

Therefore, the cost of foundation is determined by the following independent variables: W_M , L_M , f , and n .

A summary of the cost study is shown in Table 1.

3.3. Relationship between dependent and independent variables

The major cost elements involved in product price are direct material, direct labor and tooling. These elements constitute the primary cost of a production [36]. According to [36], a typical manufacturing cost breakdown involves: direct material 20%, and direct labor and tooling 9.6% of selling price. Depending on the type of manufacturing, labor or tooling can represent the main cost [37]. In this study we consider only the primary cost. Additional cost elements such as factory expenses, engineering costs, administrative costs, profit, etc., are not considered.

Labor and tooling costs included in the manufacturing of the sub-components are as follows: (i) cutting, (ii) drilling, (iii) edge grinding, (iv) welding, (v) steel surface preparation, (vi) steel surface protection, (vii) machining of the stainless steel tube, (viii) machining of the carbon steel bar, (ix) metal forming, (x) polishing of stainless steel sheets. All the cost functions needed to develop the CER are listed in Table 2.

3.3.1. Fixed structure costs

The material costs of the fixed structure include: material costs of the steel square hollow sections, electrode consumption, and costs of galvanizing process. The labor and tooling costs include: (i), (ii), (iii), (iv), (v), and (vi).

The primary cost of the fixed structure can be calculated using the cost function (c_1), where C_{FS} is the primary cost (€), W_{FS} is the total weight (kg), and k^{St} is the structure cost factor including material, labor, and tooling (€/kg).

3.3.2. Mobile structure costs

The mobile structure consists of a structure and a rail support.

The material costs of the installation rail support include: material costs of the rail support, and electrodes consumption. The labor and tooling costs include: (i), (iii), (iv), and (v).

The primary cost of the mobile structure can be calculated using the cost function (c_2), where C_{MS} is the primary cost (€), W_{MS} is the structure total weight (kg), k^{St} is the structure cost factor (€/kg), L_{rail} is the length of the rail support (m), and k^R is the installation rail support cost factor including material, labor, and tooling (€/m).

Table 1
Cost parameters and independent variables.

Element	Cost parameters	Ind. variables
Fixed str.	$W_{FS} = W_{FS}^U \cdot L_{FS}$ $L_{FS} = 2 \cdot W_M \cdot (1 + 2.15 \cdot n) + 3 \cdot L_M +$ $+ 4 \cdot \sqrt{2 \cdot \left(\frac{L_M}{2}\right)^2 + 1.5 \cdot L_M + (1.5)^2}$	W_M, L_M, n
Mobile str.	$W_{MS} = W_{MS}^U \cdot L_{MS}$ $L_{MS} = 2 \cdot (W_M \cdot (1 + 2.15 \cdot n) + L_M)$ $L_{rail} = 2 \cdot W_M \cdot (1 + 2.15 \cdot n)$	W_M, L_M, n
Movem. unit		W_M, L_M, L_a, f, n
Mirror unit	$A_{mirror} = W_M \cdot L_M$ $A_{frame} = W_M \cdot L_M$ $L_{shaft} = L_M$	W_M, L_M
Second. refl.	$W_{AT} = W_{AT}^U \cdot L_{AT} = W_{MS}^U \cdot 2 \cdot L_a$ $A_{CR} = 3.40 \cdot L_a \cdot W_M$ $A_{GC} = 2.4 \cdot L_a \cdot W_M$ $W_{SRSS} = W_{SRSS}^U \cdot (L_a + 2.4 \cdot W_M)$ $A_{PC} = 3.40 \cdot L_a \cdot W_M$ $L_{shaft\ SRS} = W_M \cdot (1 + 2.15 \cdot n)$	W_M, L_M, L_a, n
Tracking syst.		Configuration
Assembly		W_M, L_M, f, n
Foundation		W_M, L_M, f, n

3.3.3. Movement system costs

The material costs of each movement unit include: bearings, pinion gear, roller chain, stainless steel tube, stainless steel plate, and carbon steel bar. The labor and tooling costs include: (i), (ii), (iii), (iv), (v), (vii), and (viii).

The total number of movement units required by the SSLFR is equal to $(2 \cdot n + a)$, where a is a constant that can take the following values: $a = 1$ (configurations without longitudinal movements), $a = 2$ (configurations with one longitudinal movement), and $a = 3$ (configurations with two longitudinal movements).

The primary cost of the movement system can be calculated using the cost function (c_3), where C_{MoS} is the primary cost (€), and k^{MoU} is the movement unit cost factor including material, labor, and tooling (€/unit).

3.3.4. Mirror system costs

The material costs of each mirror unit include: mirror, galvanized steel sheet, galvanized steel tube, industrial adhesive, and stainless steel rivets. The labor and tooling costs include: (i), (ii), (iii), and (ix).

The total number of mirror units is equal to $(2 \cdot n + 1)$. The primary cost of the mirror units can be calculated using the cost function (c_4), where C_{MiS} is the primary cost (€), and k^{MiU} is the mirror unit cost factor including material, labor, and tooling (€/unit). k^{MiU} is given by:

$$k^{MiU} = A_{mirror} \cdot k^{mirror} + A_{frame} \cdot k^{frame} + L_{shaft} \cdot k^{shaft\ Mi} \quad (25)$$

where k^{mirror} is the mirror cost factor (€/m²), k^{frame} is the frame cost factor (€/m²), and $k^{shaft\ Mi}$ is the mirror shaft cost factor (€/m).

3.3.5. Secondary reflector system costs

The material costs of the secondary reflector system include: carbon steel tube, stainless steel sheet, glass wool, steel square hollow section, aluminum sheet, electrodes consumption, and galvanizing process. The labor and tooling costs include: (i), (ii), (iii), (iv), (v), (ix), and (x).

The primary cost of the secondary reflector system can be calculated using the cost function (c_5), where C_{SRS} is the primary cost (€), k^{AT} is the absorber tube cost factor (€/kg), k^{CR} is the receiver cavity cost factor (€/m²), k^I is the insulation cost factor (€/m²), k^{GC} is the glass covering cost factor (€/m²), k^{St} is the structure cost factor (€/kg), k^{PC} is the protective casing cost factor (€/m²), and $k^{shaft\ SRS}$ is the shaft cost factor of the secondary reflector system (€/m).

3.3.6. Tracking system costs

The costs of the tracking system include: stepper motors, stepper motor drivers, raspberry pi controller, and sensors. The primary cost of the tracking system can be calculated using the cost function (c_6), where C_{TS} is the primary cost (€), k^{MD} is the cost factor of the stepper motor and driver (€), k^C is the cost factor of the controller (€), and k^{Se} is the cost factor of the sensors (€).

3.3.7. Assembly costs

The assembly cost consists of labor and tooling cost. This cost depends on the number of sub-components of the SSLFR. Therefore, the greater n , the higher the cost. Since these costs are subject to a great uncertainty, they have to be estimated based on experience of other similar projects.

The primary assembly cost can be calculated using the cost function (c_7), where C_A is the primary cost (€), and k^A is the assembly cost factor (€/unit).

Table 2
Costs functions.

Element	Cost function	
Fixed structure	$C_{FS} = W_{FS} \cdot k^{St}$	(c ₁)
Mobile structure	$C_{MS} = W_{MS} \cdot k^{St} + L_{rail} \cdot k^R$	(c ₂)
Movement system	$C_{MoS} = (2 \cdot n + a) \cdot k^{MoU}$	(c ₃)
Mirror system	$C_{MiS} = (2 \cdot n + 1) \cdot k^{MiU}$	(c ₄)
Secondary reflector	$C_{SRS} = W_{AT} \cdot k^{AT} + A_{CR} \cdot k^{CR} + A_I \cdot k^I + A_{GC} \cdot k^{GC} + W_{SRS} \cdot k^{St} + A_{PC} \cdot k^{PC} + L_{shaft\ SRS} \cdot k^{shaft\ SRS}$	(c ₅)
Tracking system	$C_{TS} = a \cdot k^{MD} + k^C + k^{Se}$	(c ₆)
Assembly	$C_A = (2 \cdot n + a) \cdot k^A$	(c ₇)
Foundation	$C_F = V_F \cdot k^F$	(c ₈)

3.3.8. Foundation costs

The material costs of the foundation consists of the concrete cost. The labor and tooling costs include: concreting, consolidation, and curing. The primary foundation cost can be calculated using the cost function (c₈), where C_F is the primary cost (€), V_F is the foundation volume (m³), and k^F is the foundation cost factor (€/m³).

3.3.9. Total manufacturing cost

The total primary cost C_T of an SSLFR is given by the sum of eight individual cost functions:

$$C_T = C_{FS} + C_{MS} + C_{MoS} + C_{MiS} + C_{SRS} + C_{TS} + C_A + C_F \quad (26)$$

4. Numerical example

This section presents, using the proposed approach, a numerical example with the cost estimation of the SSLFR prototype shown in Fig. 1.

The estimation of the primary cost is not an exact science, so experience represents a key factor. There are many commercial software tools available for cost estimation [38]. In this work, we have used Costimator Cost Estimating Software [39] to determine the cost parameters. In addition, these costs have also been validated by a manufacturing company [40] located in Asturias (Spain). We consider the manufacturing of a single SSLFR and labor costs are given for skilled workers. The cost and geometric parameters of the SSLFR are listed in Table 3.

The calculation of the primary cost is shown in Table 4. The sub-components that most influence the cost of the SSLFR are the movement units, followed by the secondary reflector system. The independent variable that most influences the cost of the SSLFR is the number of mirrors n.

Table 3
Cost and geometric parameters.

Param.	Value	Param.	Value	Param.	Value
k St	4.53 (€/kg)	k ^I	50 (€/m ²)	k ^F	100 (€/m ³)
k ^R	29 (€/m)	k ^{GC}	60 (€/m ²)	n	12
k ^{MoU}	53 (€/unit)	k ^{PC}	600 (€/m ²)	W _M	0.06 (m)
k ^{mirror}	54.83 (€/m ²)	k ^{shaft SRS}	3 (€/m)	L _M	2.00 (m)
k ^{frame}	103.65 (€/m ²)	k ^{MD}	212 (€)	f	1.50 (m)
k ^{shaft Mi}	2.80 (€/m)	k ^C	100 (€)	L _a	2.00 (m)
k ^{AT}	20 (€/kg)	k ^{Se}	200 (€)	Config.	C ₉
k ^{CR}	1588 (€/m ²)	k ^A	12 (€/unit)	a	3

Table 4
Primary cost.

Cost	Value (€)	%
C _{FS}	811.22	13.86
C _{MS}	262.92	4.49
C _{MoS}	1431.00	24.44
C _{MiS}	615.44	10.51
C _{SRS}	1335.74	22.82
C _{TS}	936.00	16.00
C _A	324.00	5.53
C _F	137.20	2.34
Total:C_T	5851.40	100

4.1. Uncertainty analysis

This subsection focuses on how to quantify uncertainty for CERs. The two classic main sources of uncertainty (excluding external factors) are: input uncertainty and model uncertainty. As the CER in this study is not derived from regression analysis, let us focus solely on input uncertainty. The reason for this is clear: when estimating the primary costs, raw material consumptions and raw material prices may fluctuate within a certain range, so it is recommendable to add uncertainty analysis when estimating costs.

A highly suitable approach for addressing inherent cost input data uncertainties is stochastic analysis [41]. In recent decades (see, for example [42] and even more recently [43]), Monte Carlo simulation has constituted a very widely used method for performing this probabilistic analysis. In this paper, we use a number of Excel spreadsheet to perform Monte Carlo simulations using the cost input data.

The variability present in the input data of the cost parameters can be defined using different probability distributions. The following distributions for the input parameters can be found in the literature [44]: (i) uniform probability distribution; (ii) triangular probability distribution; (iii) normal probability distribution; (iv) lognormal probability distribution; and (v) author-assigned probability distribution for each input parameter.

Unfortunately, those different types of probability distributions cannot be experimentally validated due to lack of publicly available data. Hence, choosing the most appropriate probability distribution for each cost parameter is constrained by the available data and the variability present in the data. To deal with the uncertainty associated with cost, we analyzed the evolution of prices, direct

Table 5
Evolution of Cost parameters.

Parameter		June 2016	June 2017	June 2018
k St	(€/kg)	4.29	4.53	4.80
k ^R	(€/m)	27.45	29	30.71
k ^{MoU}	(€/unit)	50.16	53	56.12
k ^{mirror}	(€/m ²)	51.89	54.83	58.06
k ^{frame}	(€/m ²)	98.10	103.65	109.75
k ^{shaft Mi}	(€/m)	2.65	2.8	2.96
k ^{AT}	(€/kg)	18.93	20	21.18
k ^{CR}	(€/m ²)	1523.15	1588	1659.75
k ^I	(€/m ²)	47.32	50	52.94
k ^{GC}	(€/m ²)	58.22	60	61.86
k ^{PC}	(€/m ²)	567.85	600	635.31
k ^{shaft SRS}	(€/m)	2.84	3	3.18
k ^{MD}	(€)	207.46	212	216.59
k ^C	(€)	97.86	100	102.15
k ^{Se}	(€)	195.73	200	204.31
k ^A	(€/unit)	11.89	12	12.13
k ^F	(€/m ³)	97.82	100	102.31

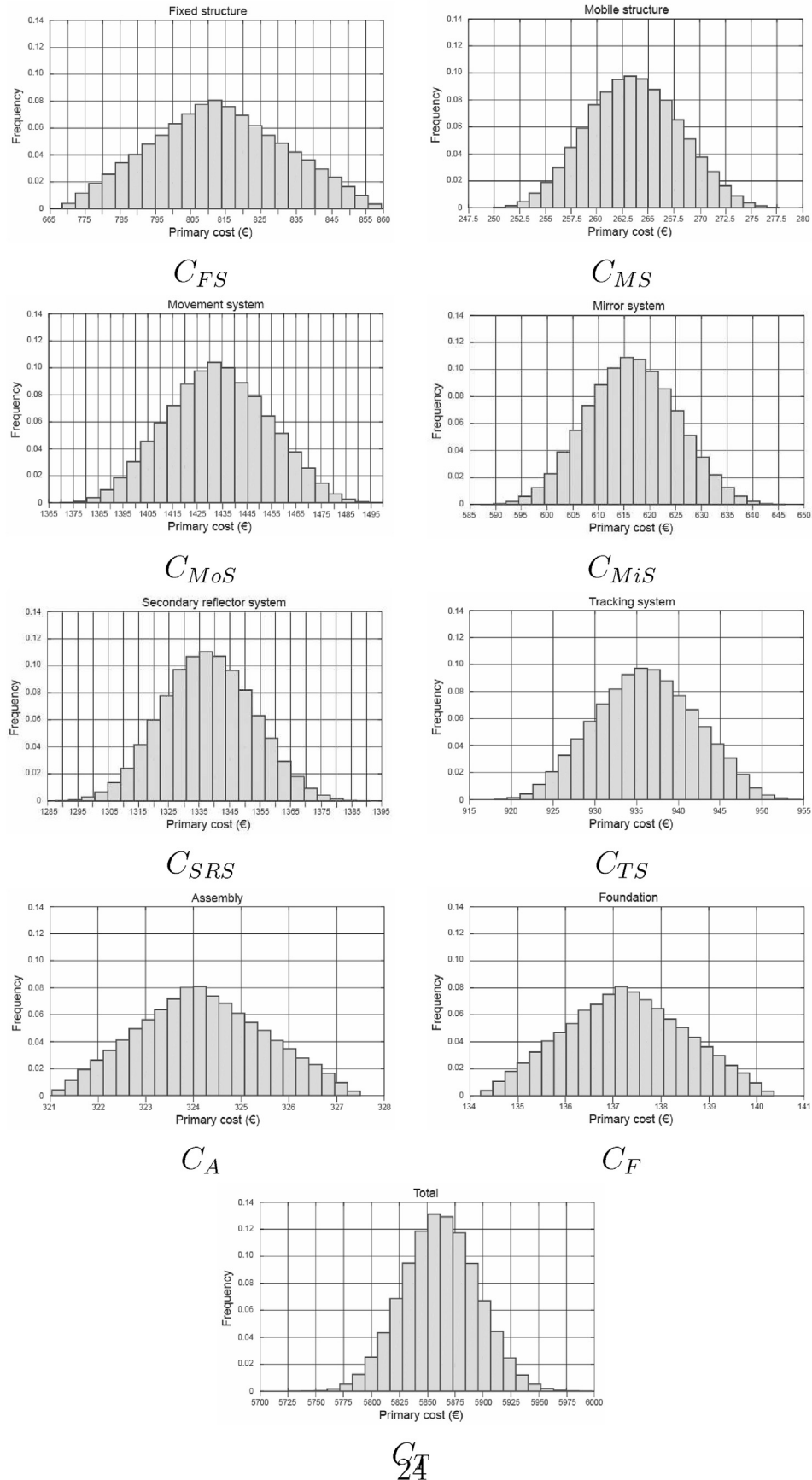


Fig. 11. Histograms of the primary costs and the total cost.

Table 6
Representative values of the simulation.

Parameter	Value
Mean	5861.90
Standard Deviation	33.22
Median	5861.70
Variance	1103.50
Rank	270.4
Minimum	5729.80
Maximum	6000.20

materials and direct labour over several years. To analyse the evolution of costs due to direct materials, we used the price indexes provided by MEPS (International) LTD. This company is a leading consultancy firm operating worldwide in the steel industry [45]. This organisation started out as a consultancy firm, mainly providing services to the steel industry. They started publishing in 1984, retaining the initials MEPS in the new company name MEPS (International) Ltd. To analyse the evolution of the direct labour costs, we used the metal-industry agreement for the north of Spain [46,47]. Table 5 presents the cost parameters for the three years under study.

Due to ambiguity in the probability distribution of the input parameters, following [48] and in order to emphasize the likely value of 2017 in the Monte Carlo simulation, a triangular distribution was selected that allows a high probability for the likely value. As stated above, the uncertainty analysis was performed using Microsoft Excel, where input data for all the input parameters were randomly generated according to their triangular probability distributions. The simulations were run for 100,000 trials.

Histograms are a common way to display the results of uncertainty analysis. Fig. 11 shows the histograms corresponding to the primary costs shown in Table 5 and also the histogram corresponding to the total cost of the SSLFR. The main values of the Monte Carlo simulation performed over the total cost, using 100,000 random inputs and following the distributions for the 17 items, is shown in Table 6.

The Monte Carlo simulation thus performed indicates that the most likely values are close to the values obtained in the previous section in which a deterministic methodology with the most probable inputs (see Table 3) was used. This is consistent with the use of triangular distributions, which allows emphasising the high probability of the likely values and therefore the results are close to the deterministic values.

5. Conclusions

A method for estimating the cost of an SSLFR has been presented. A cost estimating relationship has been developed by analyzing in detail the manufacturing processes of the SSLFR, its parameters, and sub-components. As a result of this analysis, the SSLFR has been divided into 8 sub-components: fixed and mobile structures, movement units, mirror units, secondary reflector system, tracking system, assembly, and foundation. These sub-components are described in detail and designed using Autodesk Inventor, specifying manufacturing materials and processes. The study includes a full stress analysis of the sub-components, considering self weight, snow loads, and wind loads. For each sub-component an estimate of the primary costs is presented and also a relationship between the cost and the geometric parameters of the SSLFR (W_M , L_M and n). Material, labor, and tooling costs are calculated by defining a set of cost factors. A limitation of the present study that should be borne in mind is that the values of these cost factors depend on the country where the equipment is

manufactured. A numerical example is shown, where the cost factors are determined using a commercial cost estimation software tool. Additionally, the value of these cost factors were validated by a manufacturing company located in Asturias (Spain). Another limitation of the study is related to the dimensions of the SSLFR. The values considered for W_M , L_M and n are based on the dimensions of the prototype and are suitable to maximize the energy obtained. These values allow a certain amount of variation, but if these dimensions were to vary significantly, the cost parameters would have to be recalculated.

The calculated costs show that the movement units are the sub-components that most influence the total cost of the SSLFR. Moreover, the independent variable that most influences the cost of the SSLFR is the number of mirrors (n). With regard to possible future work, this study can serve as a basis to design an SSLFR so that the maximum energy absorbed is obtained with the minimum manufacturing cost.

Acknowledgments

We wish to thank M. F. Fanjul, head of the vocational training school (CIFP-Mantenimiento y Servicios a la Producción) in La Felguera, Asturias, Spain, and the teachers L. Rodríguez and F. Salguero for their work on the building of the prototype for the design presented in this paper. Also, we wish to thank I. Díaz, head of the Talleres Metálicos Alto Nalón S.L. for his contribution in this paper.

References

- [1] IRENA, International Renewable Energy Agency, Report: Solar Heat for Industrial Processes, 2015.
- [2] Directive 2010/31/EC, On the Energy Performance of Buildings, 2010.
- [3] T. Sultana, G.L. Morrison, G. Rosengarten, Thermal performance of a novel rooftop solar micro-concentrating collector, Sol. Energy 86 (2012) 1992–2000.
- [4] T. Sultana, G.L. Morrison, R.A. Taylor, G. Rosengarten, Numerical and experimental study of a solar micro concentrating collector, Sol. Energy 112 (2015) 20–29.
- [5] G. Mokhtar, B. Boussad, S. Noureddine, A linear Fresnel reflector as a solar system for heating water: theoretical and experimental study, Case Stud. Therm. Eng. Case 8 (2016) 176–186.
- [6] P. Bermejo, F.J. Pino, F. Rosa, Solar absorption cooling plant in Seville, Sol. Energy 84 (2010) 1503–1512.
- [7] F.J. Pino, R. Caro, F. Rosa, J. Guerra, Experimental validation of an optical and thermal model of a linear Fresnel collector system, Appl. Therm. Eng. 50 (2013) 1463–1471.
- [8] M.A. Serag-Eldin, Thermal design of a roof-mounted CLFR collection system for a desert absorption chiller, Int. J. Sustain. Energy 33 (2014) 506–524.
- [9] N. Velázquez, O. García-Valladares, D. Saucedá, R. Beltrán, Numerical simulation of a linear Fresnel reflector concentrator used as direct generator in a Solar-GAX cycle, Energy Convers. Manag. 51 (2010) 434–445.
- [10] R. Singh, Modeling and Performance Analysis of Linear Fresnel Collector for Process Heat Generation for Ice Cream Factory in Konya, MS Thesis, Middle East Technical University, 2017.
- [11] A. Häberle, M. Berger, F. Luginsland, C. Zahler, M. Baitsch, H. Henning, M. Rommel, Linear concentrating Fresnel collector for process heat applications. Solar Paces, in: 13th International Symposium on Concentrating Solar Power and Chemical Energy Technologies, June 20–23, Sevilla, Spain, 2006.
- [12] J. Rawlins, M. Ashcroft, Report: Small Scale Concentrated Solar Power – a Review of Current Activity and Potential to Accelerate Employment, Carbon Trust, 2013.
- [13] A. Barbón, J.A. Sánchez-Rodríguez, L. Bayón, N. Barbón, Development of a fiber daylighting system based on a small scale linear Fresnel reflector: theoretical elements, Appl. Energy 212 (2018) 733–745.
- [14] A. Barbón, N. Barbón, L. Bayón, J.A. Otero, Optimization of the length and position of the absorber tube in small-scale linear Fresnel concentrators, Renew. Energy 99 (2016) 986–995.
- [15] A. Barbón, N. Barbón, L. Bayón, J.A. Sánchez-Rodríguez, Optimization of the distribution of small scale linear Fresnel reflectors on roofs of urban buildings, Appl. Math. Model. 59 (2018) 233–250.
- [16] A. Niazi, J.S. Dai, S. Balabani, L. Seneviratne, Product cost estimation: technique classification and methodology review, J. Manuf. Sci. Eng. 128 (2) (2006) 563–575.
- [17] L. Qian, D. Ben-Arieh, Parametric cost estimation based on activity-based costing: a case study for design and development of rotational parts, Int. J. Prod. Econ. 113 (2008) 805–818.

- [18] OEPM. Oficina Española de Patentes y Marcas. [cited 2017, February 14th].
- [19] A. Barbón, N. Barbón, L. Bayón, J.A. Otero, Theoretical elements for the design of a small scale linear Fresnel reflector: frontal and lateral views, *Sol. Energy* 132 (2016) 188–202.
- [20] G. Morin, J. Dersch, W. Platzer, M. Eck, A. Häberle, Comparison of linear Fresnel and parabolic trough collector power plants, *Sol. Energy* 86 (2012) 1–12.
- [21] S.S. Mathur, T.C. Kandpal, B.S. Negi, Optical design and concentration characteristics of linear Fresnel reflector solar concentrators-I. Mirror elements of varying width, *Energy Convers. Manag.* 31 (3) (1991) 205–219.
- [22] S.S. Mathur, T.C. Kandpal, B.S. Negi, Optical design and concentration characteristics of linear Fresnel reflector solar concentrators- II. Mirror elements of equal width, *Energy Convers. Manag.* 31 (3) (1991) 221–232.
- [23] P. Sandborn, *Cost Analysis of Electronic Systems*, World Scientific Publishing Co. Ptr. Ltd., Singapore, 2013.
- [24] A. Barbón, N. Barbón, L. Bayón, J.A. Sánchez-Rodríguez, Parametric study of the small scale linear Fresnel reflector, *Renew. Energy* 116 (2018) 64–74.
- [25] J. Zheng, J. Yan, J. Pei, G. Liu, Solar Tracking Error Analysis of Fresnel Reflector, Hindawi Publishing Corporation The Scientific World Journal, 2014, p. 6. Article ID 834392.
- [26] Y. Zhu, J. Shi, Y. Li, L. Wang, Q. Huang, G. Xu, Design and thermal performances of a scalable linear Fresnel reflector solar system, *Energy Convers. Manag.* 146 (2017) 174–181.
- [27] I. Reda, A. Andreas, Solar position algorithm for solar radiation applications, *Sol. Energy* 76 (2004) 577–589.
- [28] J.J. Michalsky, The astronomical Almanac's algorithm for approximate solar position (1950–2050), *Sol. Energy* 40 (1988) 227–235.
- [29] M. Blanco-Muriel, D.C. Alarcon-Padilla, T. Lopea-Moratalla, M. Lara-Coira, Computing the solar vector, *Sol. Energy* 70 (2001) 431–441.
- [30] R. Grena, An algorithm for the computation of the solar position, *Sol. Energy* 82 (2008) 462–470.
- [31] R. Grena, Five new algorithms for the computation of sun position from 2010 to 2110, *Sol. Energy* 86 (5) (2012) 1323–1337.
- [32] S. Malav, S. Vadhera, Hardware implementation of solar tracking system using a stepper motor, in: *IEEE International Conference on Energy, Power and Environment (ICEPE)*, IEEE, 2015.
- [33] X. Jin, G. Xu, R. Zhou, X. Luo, Y. Quan, A sun tracking system design for a large dish solar concentrator, *Int. J. Clean Coal Energy* 2 (2013) 16–20.
- [34] R. Abd Rahim, M.N.S. Zainudin, M.M. Ismail, M.A. Othman, Image-based solar tracker using raspberry pi, *J. Multidiscip. Eng. Sci. Technol. (JMEST)* 1 (5) (2014) 369–373.
- [35] L.E. Palomino, G. Alexandre, Solar radiation monitoring using electronic embedded system raspberry pi database connection MySQL, ubidots and TCS-230 sensor, in: *IEEE Conference on Electrical, Electronics Engineering, Information and Communication Technologies (CHILECON)*, IEEE, 2015.
- [36] J.T. Black, *The Design of the Factory with a Future*, McGraw Hill, Inc., New York, 1991.
- [37] G. Molcho, A. Cristal, M. Shpitalni, Part cost estimation at early design phase, *CIRP Ann. - Manuf. Technol.* 63 (2014) 153–156.
- [38] K.H. Chang, *Product Manufacturing and Cost Estimating Using CAD/CAE*, The Computer Aided Engineering Design Series, Elsevier, 2013, pp. 270–273 (Chapter 6).
- [39] H.D.S. Budiono, G. Kiswanto, T.P. Soemardi, Method and model development for manufacturing cost estimation during the early design phase related to the complexity of the machining processes, *Int. J. Technol.* 2 (2014) 183–192.
- [40] TMAN, Talleres Metálicos Alto Nalón, 2018. Available from: <http://www.talleressaltonalon.com/> (Accessed on: 7 August 2018).
- [41] P.R. Garvey, S.A. Book, R.P. Covert, *Probability Methods for Cost Uncertainty Analysis: a Systems Engineering Perspective*, second ed., Chapman and Hall/CRC, New York, 2016.
- [42] P.F. Dienemann, *Estimating Cost Uncertainty Using Monte Carlo Techniques*, RAND Corporation, Santa Monica, California, 1966. No. RAND-RM-4854-PR.
- [43] P.R.G. Couto, J.C. Damasceno, S. Pinheiro de Oliveira, Monte Carlo Simulations Applied to Uncertainty in Measurement, Theory and Applications of Monte Carlo Simulations, InTech, 2013.
- [44] N.R. Baral, C. Quiroz-Arita, T.H. Bradley, Uncertainties in corn stover feedstock supply logistics cost and life-cycle greenhouse gas emissions for butanol production, *Appl. Energy* 208 (2017) 1343–1356.
- [45] MEPS, MEPS (International) LTD, 2018. Available from: <http://www.meps.co.uk/> (Accessed on: 7 August 2018).
- [46] BOPA (Boletín Oficial del Principado de Asturias), núm. 108 de 12-v-2017. Available from: <https://sede.asturias.es/bopa/2017/05/12/2017-04836.pdf>.
- [47] BOPA (Boletín Oficial del Principado de Asturias), núm. 25 de 31-i-2018. Available from: <https://sede.asturias.es/bopa/2018/01/31/2018-00607.pdf>.
- [48] M.A. Meybodi, A.C. Beath, Impact of cost uncertainties and solar data variations on the economics of central receiver solar power plants: an Australian case study, *Renew. Energy* 93 (2016) 510–524.